Astronomy & Astrophysics manuscript no.
(will be inserted by hand later)

SBS 0335–052 E and W: implications of new broad-band and Hα photometry

S.A. Pustilnik[1,3], A.G. Pramskij[1,3], and A.Y. Kniazev[1,2,3]

[1] Special Astrophysical Observatory, Nizhnij Arkhyz, Karachai-Circassia, 369167, Russia
[2] Max Planck Institut für Astronomie, Königstuhl 17, D-69117, Heidelberg, Germany
[3] Isaac Newton Institute of Chile, SAO Branch

Received 22 July 2003; accepted 2 March 2004

Abstract. We present the results of deep multicolour CCD imaging with the SAO RAS 6 m telescope of the pair of extremely metal-deficient gas-rich dwarf galaxies SBS 0335–052 E and W. The total magnitudes in U, B, V, R and I bands and the integrated fluxes of Hα emission are measured for both galaxies, and their integrated colours are derived. The analysis of their surface brightness (SB) distributions is performed with the use of the azimuthally-averaged SB profiles. The latter were modeled by the central Gaussian component and the underlying exponential 'disk', mainly contributing in the outermost, very low SB regions. The colours of these LSB components are used to estimate the age of the oldest visible stellar population. For the interpretation of the observed LSB colours their contamination by the nebular emission of ionized gas is accounted for by the use of the distribution of Hα flux. We compare the derived 'gas-free' colours with the colours predicted by the evolution synthesis models from the PEGASE.2 package, considering three SF histories: a) instantaneous starburst, b) continuous star formation with constant SFR, and c) continuous exponentially fading SF (e-fold time of 3 Gyr). We conclude that the 'gas-free' colours of the LSB component of the Eastern galaxy can be best consistent with the instantaneous starburst population (ages of $\lesssim$100 Myr). Models with continuous SF give less consistent results, but can be considered as acceptable. For such scenarios, the 'gas-free' colours require ages of $\lesssim$400 Myr. For the Western galaxy, the situation is in general similar. But the colour $(V-R)$ appears to be quite red and implies a significantly older component. We briefly discuss the possible evolution sequence between SBS 0335–052, HI 1225+01 and other extremely metal-deficient galaxies based on the merger scenario.

Key words. galaxies: starburst – galaxies: photometry – galaxies: evolution – galaxies: individual (SBS 0335–052 E and W)

1. Introduction

The system SBS 0335–052 E,W – a unique pair of dwarf galaxies with the projected separation of 22 kpc, and the lowest (together with I Zw 18) ionized gas oxygen abundances known (1/42 and 1/50 of solar value, respectively)[1] was first described by Izotov et al. (1990), Pustilnik et al. (1997) and Lipovetsky et al. (1999). This galaxy pair has been intensively studied over the last 13 years, and there are about 40 papers devoted to various aspects of this multiwavelength and multimethod attack. Here we concentrate mainly on its photometric properties, related to its age, postponing the discussion of some other properties of this system to Sect. 5.

The very blue $(V-I)$ colour of SBS 0335–052 E was first derived from the HST photometry by Thuan et al. (1997). Also, in this work the starburst was resolved into several superstar clusters. In papers by Izotov et al. (1997, 2001) it was shown that the Hα emission of this galaxy is very extended. It was argued that this nebular emission is mixed with and well diluted by the radiation of the sea of unresolved underlying late B and early A stars.

The detailed analysis of the broad-band surface photometry of this galaxy coupled with the high S/N long-slit spectra was presented by Papaderos et al. (1998). The broad-band colours of the LSB halo were modeled by the mixture of stellar and gas emission. The observed nebular emission was directly accounted for in this analysis for the region covered by the long-slit strip of $1''\times6''$. These authors concluded that their data indicate no detectable contribution of old stars to the LSB underlying halo. However, Kunth & Östlin (2001) questioned their results, mainly due to the use of the different models for colour evolution.

Send offprint requests to: S. Pustilnik, e-mail: sap@sao.ru

[1] The solar value is accepted here as 12+log(O/H)=8.92 (Anders & Grevesse 1989) to discus the oxygen abundance in the same system as other authors. In fact, recent data show that this value seems to be 0.2 dex lower (Prieto et al. 2001).

The extremely low oxygen abundance of the Western galaxy was determined by Lipovetsky et al. (1999). Its first R, I photometry was also presented in this paper. Papaderos et al. (1998) presented the detailed analysis of the total and SB broad-band photometry of this galaxy. While their photometry was rather deep, the compactness and faintness of this galaxy prevented to perform the analysis of its evolution status. Near IR data on SBS 0335–052 E and W colours were presented by Vanzi et al. (2000). Despite that observations in the NIR range are the most sensitive to the presence of an old stellar population, only the upper limit (∼15%) on the contribution of its NIR radiation in the Eastern galaxy was derived.

Up to now, the absence of very deep optical photometry supported by a deep imaging in nebular emission lines (first of all, in Hα), or even better with full two-dimensional spectrophotometry, prevented us from getting reliable colours of an underlying "old" stellar population in this type of object. The essence of this new step, performed with the SAO 6 m telescope data, is an attempt to elaborate methods for similar studies of other actively studied or recently discovered extremely metal-deficient (hereafter XMD) BCGs (e.g., Papaderos et al. 1999; Kniazev et al. 2000a, 2000b; Fricke et al. 2001; Guseva et al. 2001; Melbourne & Salzer 2002; Ugryumov et al. 2003; Pustilnik et al. 2004). A similar approach was recently realized for the analysis of the LSB underlying component in I Zw 18 by Papaderos et al. (2002). In Sect. 2 we describe the observations and their reduction. Sect. 3 presents the results of the data analysis. We further compare the derived colours with the model tracks of evolving stellar populations in Sect. 4. These results are discussed in Sect. 5. We summarize our findings and draw conclusions in Sect. 6. All distance-dependent parameters discussed in the paper are calculated with the adopted distance to the system of 54.3 Mpc. This corresponds to the scale of 263 pc in 1″.

2. Observations and data reduction

$UBVRI$ broad-band and Hα narrow-band photometry was carried out with the 6 m telescope (BTA) of the Special Astrophysical Observatory of Russian Academy of Sciences (SAO RAS) during three runs in November–December 1997 (Table 2). Observational data were obtained in the prime focus of the telescope using the 1040×1160 pixel ISD017A CCD detector, binned 2×2, with the gain 2.3 e/ADU and the resulting scale 0.274 arcsec pixel^{-1}. The broad-band U, B and V are the Johnson photometry system filters, while R and I filters are those from the Cousins system (Bessell 1990). Observations in Hα were performed in two narrow-band filters with FWHM = 85 Å, centered at λ6660 Å (Hα-line) and λ6740 Å (Hα-cont) for measurements of the Hα emission line and Hα-free continuum flux, respectively. Observations were conducted with the software package `NICE` in MIDAS[2], as described by Kniazev & Shergin (1995). The exposure times, mean values of airmass and seeings for observations in each filter are presented in Table 2. The images in each filter were obtained by summing several exposures. The individual exposures in broad-band filters (BVI), as well as those for Hα narrow filters, were conducted in a cyclic sequence ($B \Rightarrow V \Rightarrow I \Rightarrow B$). Each night we obtained bias, dark and flat-field images for primary reduction. The broad-band photometric standards were observed in the fields PG 0039+049, Feige 22, G93–48 and PG 2317+046 (Landolt 1992). For calibration of narrow-band Hα frames, we observed spectrophotometric standards BD+28°4211, Feige 11 and Feige 34 from Bohlin (1996).

Table 1. Journal of Observations

Date	Band	Exposure time [s]	Seeing [arcsec]	Airmass
(1)	(2)	(3)	(4)	(5)
09.11.1997	Hα-line	6×600	1.9	1.53
09.11.1997	Hα-cont	6×600	1.9	1.53
09.11.1997	R_c	3×120	1.9	1.55
26.11.1997	B	3×300	2.3	1.54
26.11.1997	V	3×300	2.2	1.54
26.11.1997	R_c	1×300	2.0	1.54
26.11.1997	I_c	3×300	1.9	1.54
01.12.1997	U	4×900	3.0	1.55

Standard reduction steps, including bias-subtraction, flat-field correction, removal of cosmic ray hits and absolute flux calibration were carried out using IRAF[3] and MIDAS. The aperture photometry of SBS 0335–052 E and W and of the standard stars was performed in IRAF with `APPHOT` tasks `polyphot` and `phot`. The surface brightness profiles were obtained with the `STSDAS` task `ellipse`.

3. Results

3.1. Integrated photometry

In Table 2 we present the total magnitudes and colours for the east and west galaxies of the SBS 0335–052 system. For comparison, we show in this table the same parameters derived by Thuan et al. (1997), Papaderos et al. (1998) and Lipovetsky et al. (1999). The errors of our instrumental magnitudes are very small for both east and west galaxies, less than $\sim 0\overset{m}{.}01$, and are significantly lower than the uncertainties resulting from the photometric system transformations. Therefore, despite the large difference in the

[2] MIDAS is an acronym for the European Southern Observatory package — Munich Image Data Analysis System.

[3] IRAF: the Image Reduction and Analysis Facility is distributed by the National Optical Astronomy Observatories, which is operated by the Association of Universities for Research in Astronomy, In. (AURA) under cooperative agreement with the National Science Foundation (NSF).

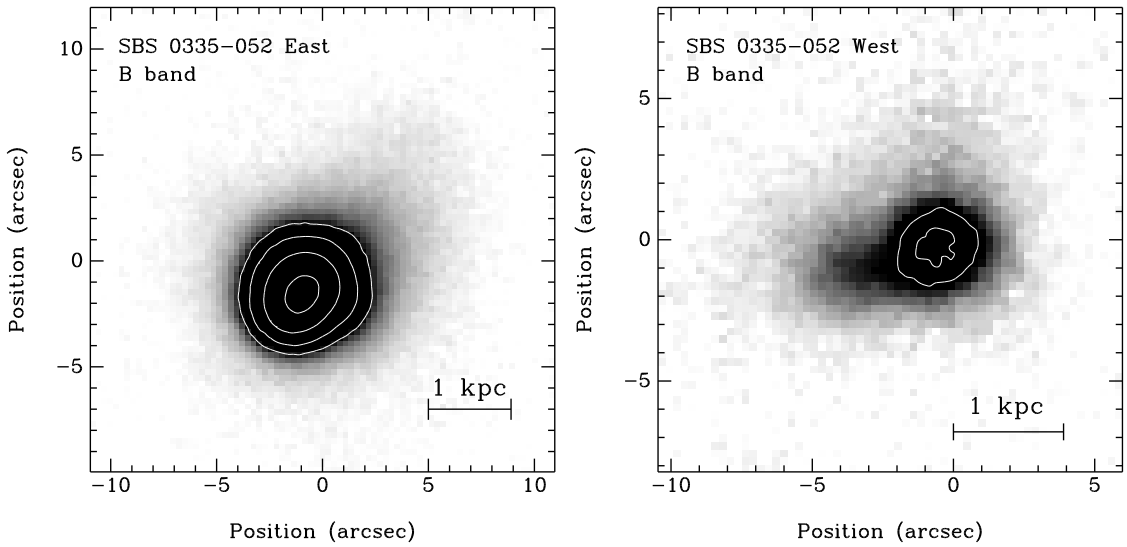

Fig. 1. BTA B-images of SBS 0335–052 East (left) and West (right) galaxies in grey-scale. The superimposed isophotes from the center outwards correspond to surface brightness levels of 19.7, 20.7, 21.7 and 22.5 mag arcsec^{-2} - for the east galaxy, and 22.3 and 22.9 mag arcsec^{-2} - for the west galaxy.

Table 2. Total magnitudes and colours

Parameter	0335−052 E	0335−052 W	Ref
$U^{\ddagger}$	16.24 ± 0.06	18.71 ± 0.06	1
	16.24 ± 0.04	18.74 ± 0.08	2
B	16.95 ± 0.03	19.14 ± 0.03	1
	16.96 ± 0.02	19.29 ± 0.07	2
V	16.65 ± 0.03	19.25 ± 0.03	1
	16.65 ± 0.01	.....	3
R	16.52 ± 0.03	18.82 ± 0.04	1
	16.57 ± 0.01	19.03 ± 0.05	4
I	16.88 ± 0.04	18.94 ± 0.04	1
	16.88 ± 0.01	19.08 ± 0.05	3,4
$(U-B)$	-0.71 ± 0.07	-0.43 ± 0.07	1
	-0.72 ± 0.05	-0.54 ± 0.10	2
$(B-V)$	0.30 ± 0.05	-0.12 ± 0.05	1
	0.31 ± 0.03	.....	2,3
$(V-R)$	0.13 ± 0.05	0.44 ± 0.05	1
	0.08 ± 0.02	.....	3,4
$(V-I)$	-0.23 ± 0.05	0.31 ± 0.05	1
	-0.23 ± 0.02	.....	3
$(R-I)$	-0.36 ± 0.05	-0.12 ± 0.05	1
	-0.35 ± 0.02	-0.05 ± 0.07	2,4
F(Hα)†	3227 ± 107	144 ± 6	1

‡ Adopted for the east galaxy equal to that in (2);
† Total flux in Hα-line in units 10^{-16} erg cm^{-2}s^{-1};
(1) – this paper; (2) – Papaderos et al. (1998);
(3) – Thuan et al. (1997); (4) – Lipovetsky et al. (1999);

total magnitudes of the east and west galaxies, the errors of their total magnitudes are very similar. For the U-band we had no photometric system parameters. We observed two standard stars, one of which was at different air mass. From these observations we estimated the extinction and the colour terms, and got the first approximation for the total U-band magnitude of the east galaxy, $0\overset{\mathrm{m}}{.}14$ brighter than that from Papaderos et al. (1998). Since the accuracy of the calibration of our U-band data was difficult to assign, we adopted the total U-band magnitude for the east galaxy as equal to that from Papaderos et al. (1998). For the west galaxy the U-magnitude was simply recalculated from the measured instrumental magnitude difference between the east and west galaxies. The difference ΔU for the west galaxy between our and the Papaderos et al. values is significantly lower than 1σ of the combined error.

In B-band our integrated magnitude of the east galaxy coincides nicely with the value of Papaderos et al (1998). For the west galaxy the difference is larger, but still acceptable, approximately within 2σ of the combined error. In the V-band there exist in the literature only integrated magnitudes for the east galaxy (Thuan et al. 1997). It exactly coincides with our measurement. The total magnitudes in R-band were published by Lipovetsky et al. (1999). Our value for the east galaxy is $0\overset{\mathrm{m}}{.}05$ brighter than theirs, but still is well consistent (within 1.7σ of the combined error). However, for the west component we measure the total magnitude to be $0\overset{\mathrm{m}}{.}21$ brighter than the value in Lipovetsky et al. (1999). This difference exceeds 3σ of the combined error ($\sigma_{\mathrm{comb}}=0\overset{\mathrm{m}}{.}064$), and indicates possible systematic effects. A similar situation, but less striking, occurs for the I-band. Again, for the east galaxy our total magnitude and that from Thuan et al. (1997) coincide completely. However, for the west galaxy, our total I-band magnitude is $0\overset{\mathrm{m}}{.}14$ brighter than that from Lipovetsky et al. (1999). The combined error for this difference is the same as for the R-band, and this difference slightly exceeds $2\sigma_{\mathrm{comb}}$.

Thus, besides R and I total magnitudes for the west galaxy, our data are consistent with previous measurements. For the latter, the difference comes from the re-

sults obtained with the Calar Alto 2.2-m telescope, with the limited photon statistics for the west galaxy (compare their reduced S/N for the west galaxy relative to that of the east galaxy). This implies that small uncertainties in the determination of the sky background could additionally affect the integrated magnitude of the west galaxy, and thus cause the slight decrease in the flux in R and I. Probably, a similar effect in the B-band can explain the difference ($0\overset{\mathrm{m}}{.}15$) of our and Papaderos et al. magnitudes for the west galaxy.

The derivation of Hα-flux could be affected by the emission lines that appeared within the Hα-cont filter passband and the small variations of the CCD detector sensitivity between the wavelengths of the two narrow filters. The former is mostly due to Hα itself in the Hα-cont filter and the He I-line λ6678 Å, which result in the decrease of the measured Hα-flux by ∼3.8% and ∼0.9%, respectively. The [S II]-lines λλ6717,6731 Å contribute ∼0.3%. Thus, the total correction of 5% to the directly measured Hα-flux was applied. The small variations of the CCD detector sensitivity between the two narrow filters are completely accounted for by observations of spectrophotometric standards in each of them. The measurements of Hα flux for the east galaxy were presented by Melnick et al. (1992) (integrated over the region of 3 arcsec^2) and for the west galaxy by Lipovetsky et al. (1999) (integrated over the region of 4 arcsec^2). Our integrated Hα flux for the east galaxy is a factor of ∼1.6 higher than that obtained by Melnick et al. (1992). For the west galaxy our integrated Hα flux is a factor of 2 higher than that obtained by Lipovetsky et al. (1999). This implies that besides the emission from the two compact knots, there is a significant contribution from more diffuse gas. The implications of the Hα luminosity data are discussed in Sect. 5.4.

3.2. Surface photometry

The B-band images of both galaxies are shown in Figure 1 for further comparison with their images in the net Hα. The results of our surface photometry are presented as the surface brightness profiles (SBPs) in Figure 2. Each of the six panels shows SBPs of both east and west galaxies in the respective broad-band and Hα filters. SBPs for the east and west galaxies are shown by filled and open squares, respectively. The Hα SBPs were transformed from the instrumental magnitudes to some conditional magnitudes using the same zero-point and colour term coefficients as for the R-band. This allows us to directly estimate the contribution of Hα into R-band flux from the plotted SBPs. For example, at $R_{\rm eff}$=6″ we have for the east galaxy $\mu_{\rm R}$ ∼24 mag arcsec^{-2}, while $\mu_{\rm H\alpha}$ ∼24.5 mag arcsec^{-2}. This implies that at this radius the flux in the Hα-line contributes 50% of the total R-band flux (accounting for R-filter transmission of ∼0.8 at the observed wavelength of Hα), or the ratio of the line and continuum fluxes within R-filter band is ∼1.0. Accounting for the equivalent width of the R-band of ∼1600 Å, this means that at $R_{\rm eff}$=6″ the mean EW(Hα) is ∼1600 Å. Similarly, at $R_{\rm eff}$=8″ we can roughly estimate the mean EW(Hα) as ∼400 Å. This immediately shows the important effect of nebular emission on the colours of the outermost LSB component.

The model fittings of the SBPs for the east and west galaxies are shown by the solid and dashed lines, respectively. We fitted their SBPs, assuming that the outer parts of both galaxies are well described by the exponential profile (kind of disk): $\mu(r) = \mu_0 + 1.086 \times r/\alpha_0$. The innermost bright region with active star formation was approximated by a Gaussian profile $\mu(r) = \mu_{\rm G} + 1.086 \times \ln 2 \times (2 \cdot r/\alpha_{\rm G})^2$, where $\alpha_{\rm G}$ is the FWHM of the Gaussian profile. Since we are mainly interested in the colours of the outermost parts of these galaxies, the exact form of the SBPs in the central bright regions is outside the scope of this study. This is natural, accounting for the modest seeing we have for these data.

The derived model parameters with their uncertainties are given in Table 3. With the scalelengths of broad-band "disk" components of 1.″7–1.″9 for east, and 1.″6–1.″7 for west galaxies, these disk-like profiles can be followed up to 4–5 scalelengths ($R_{\rm eff}$=10″ and 7–8″, respectively) reaching the surface brightness level of ∼27 mag. arcsec^{-2} in B and V, and about 1 mag brighter in U and I. The Hα SBPs can also be followed in the outer parts with the same $R_{\rm eff}$, and are more or less well described outside the bright star-forming regions by an exponential law. Since the seeing FWHM is comparable to the 'disk' scalelength, we have modeled the convolution of the found disk with its respective Gaussian to check how much the seeing affects the 'disk' parameters. The effect is small: μ_0 gets fainter by 0.05 mag, while the scalelength increases by 2%. The effect of seeing on the parameters of the central Gaussian is very large: its central brightness drops by 1.15 mag, and the FWHM increases by a factor of 1.6. Therefore we do not discuss the central Gaussian parameters below. Disk fitting for the W galaxy is further complicated by the presence of two distinct knots with a distance of ∼4″. Since the maximum effective radius to which the light of the W galaxy is followed is only ∼6–8″, in some cases (in U) it is difficult to perform a reasonable exponential fitting to the SBP.

In columns 7 and 8 of Table 3 we also present the total magnitudes of the LSB 'disk' components and those of the starburst components. The former is calculated by the standard formula for an exponential disk using the parameters μ_0 and α_0:

$$m_{\rm disk} = \mu_0 - 5.0 \times \log(\alpha_0) - 2.5 \times \log(2\pi)$$

The magnitudes of the starburst component are calculated from the total magnitudes of the galaxy in Table 2 subtracting the flux of the LSB 'disk'.

It is worth noting that the scalelengths of 'disk' components are quite close for the east and west galaxies (mean ∼1.″78 and 1.″70, respectively), while the central SB $\mu^0_{\rm B,corr}$ differ significantly. For the east galaxy this parameter is 21.07 mag arcsec^{-2}, typical of BCGs. For the west galaxy

Table 3. Model parameters of the surface brightness profiles for SBS 0335–052 E and W

Band	μ_0 mag arcsec^{-2}	α_0 arcsec	α_0 pc	μ_G mag arcsec^{-2}	α_G arcsec	m_{disk} mag	m_{burst} mag	Ref
1	2	3	4	5	6	7	8	9
Eastern galaxy								
U	20.27±0.05	1.82±0.02	468±5	20.10±0.02	3.88±0.03	16.98±0.05	17.01	1
	20.66±0.08	1.74±0.04	459±12	—	—	—	—	2
B	21.27±0.04	1.83±0.02	470±5	19.90±0.02	2.83±0.03	17.96±0.05	17.49	1
	21.38±0.05	1.74±0.03	458±8	—	—	—	—	2
V	20.72±0.05	1.72±0.02	442±5	19.46±0.03	2.56±0.03	17.55±0.05	17.28	1
	20.71±0.26	1.43	376±30	—	—	—	—	3
R	20.54±0.03	1.71±0.02	439±5	19.25±0.02	2.43±0.02	17.38±0.04	17.18	1
	21.61±0.10	2.32	610±15	—	—	—	—	2,4
I	21.24±0.08	1.89±0.04	486±10	19.43±0.03	2.38±0.03	17.86±0.09	17.44	1
	20.96±0.35	1.50	396±43	—	—	—	—	2,3
Hα	21.27±0.02	1.61±0.01	391±3	20.02±0.02	2.16±0.02	18.24±0.03	18.15	1
Western galaxy								
U	21.85±0.08	1.62±0.04	416±10	—	—	18.81±0.09	21.35	1
	22.27±0.34	1.53±0.15	402±40	—	—	—	—	2
B	22.49±0.10	1.73±0.05	445±13	23.61±0.15	2.72±0.18	19.30±0.12	21.27	1
	22.33±0.22	1.47±0.07	387±20	—	—	—	—	2
V	22.41±0.05	1.61±0.03	414±5	23.71±0.14	2.12±0.11	19.38±0.06	21.61	1
R	22.06±0.03	1.69±0.02	434±13	22.98±0.07	2.04±0.13	18.93±0.04	21.40	1
I	22.20±0.08	1.65±0.05	424±13	22.94±0.11	1.94±0.11	19.12±0.09	20.99	1
Hα	22.82±0.10	0.96±0.02	247±5	—	—	20.91±0.12	23.70	1

All values are not corrected for the Galactic extinction; Ref: (1) – Data from this paper; (2) – Papaderos et al. (1998); (3) – Thuan et al. (1997); (4) – Lipovetsky et al. (1999);

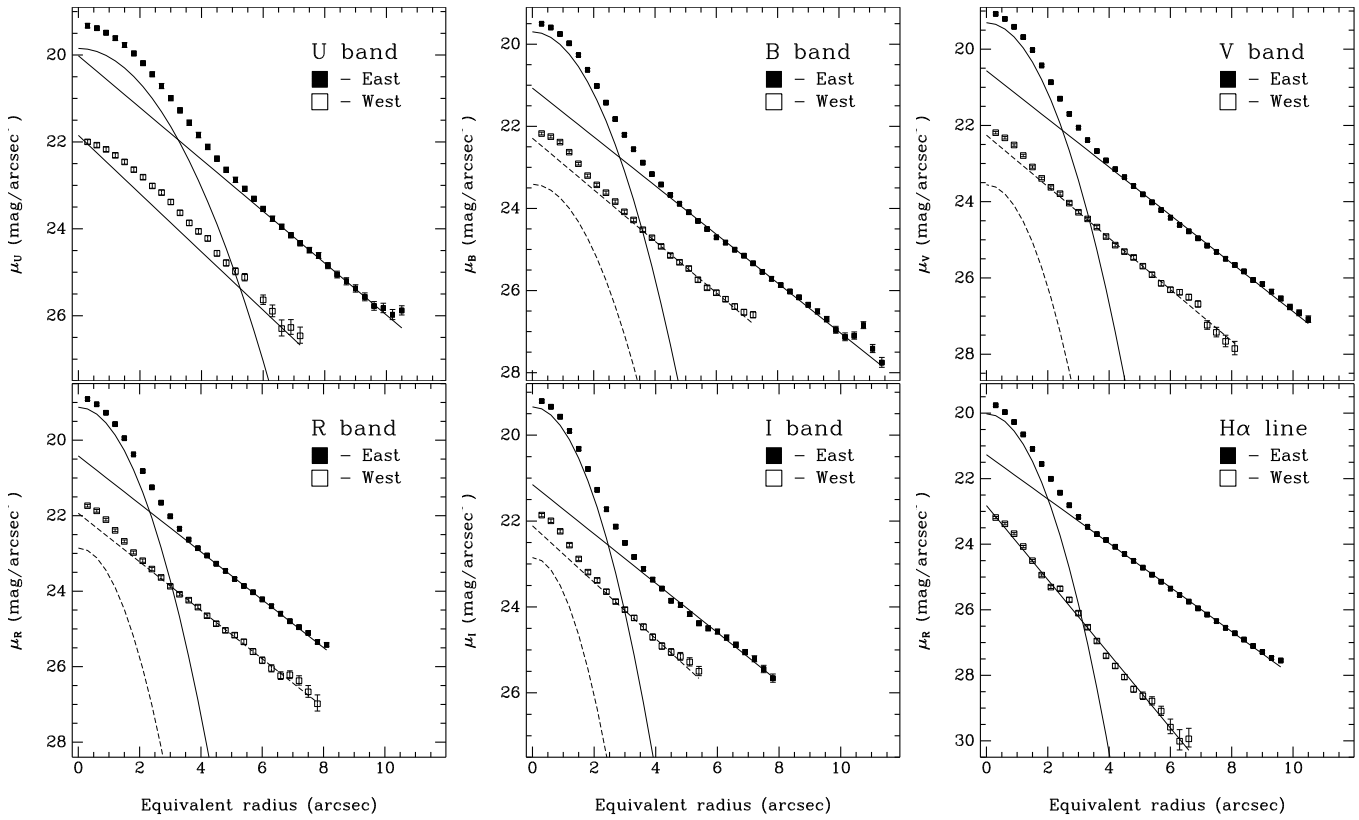

Fig. 2. Surface brightness profiles (SBPs) for SBS 0335–052 E and W. Instrumental Hα-line SBP was transformed into conditional magnitudes using the R-band photometrical coefficients. All the data are corrected for the Galactic extinction.

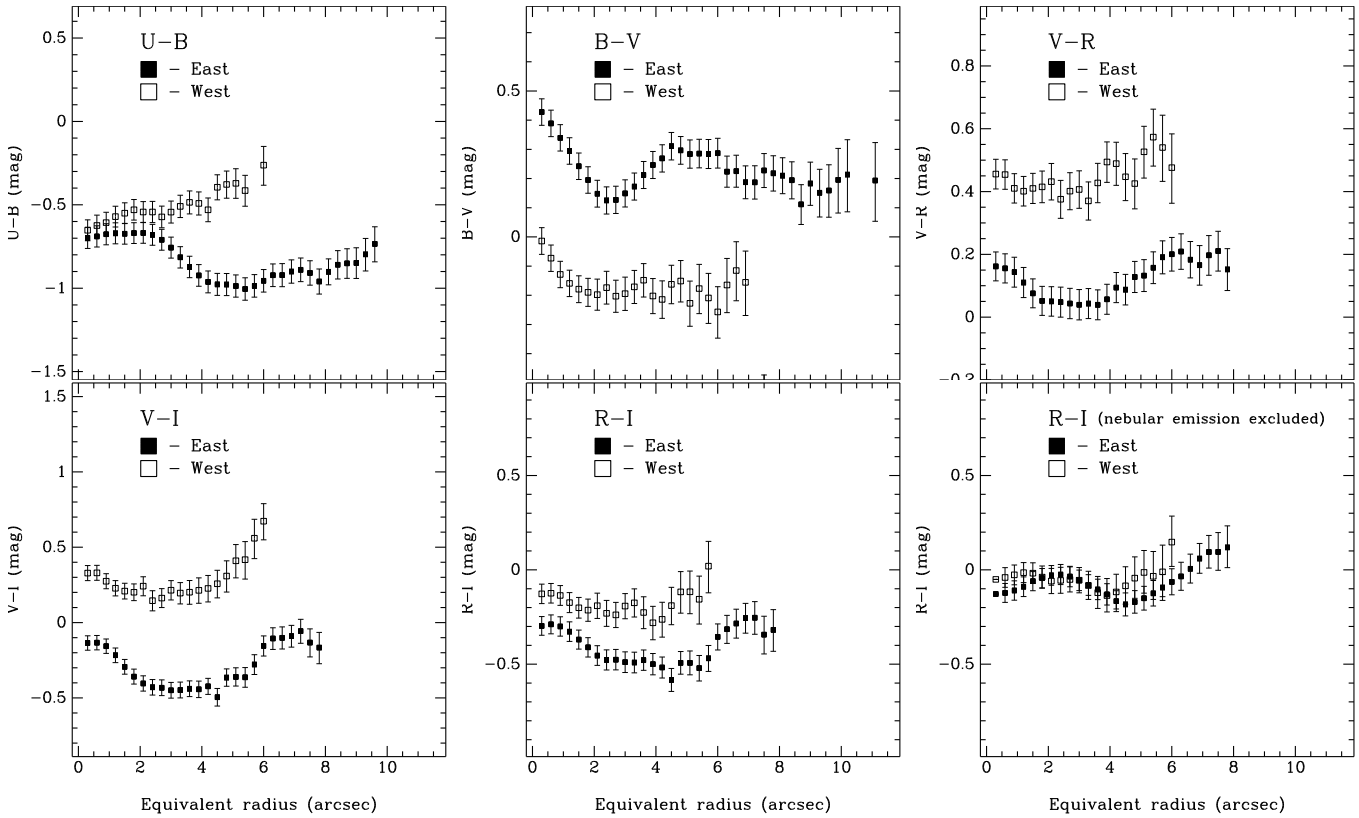

Fig. 3. Radial distributions of colours for SBS 0335–052 E and W, corrected for Galactic extinction. Only $R-I$ gas-free colour distributions are shown since they are practically independent of the model assumptions for the ionized gas parameters (see Sect. 4.1).

this parameter is 22.29 mag arcsec^{-2}, more typical of dIrr galaxies. Furthermore, the apparent strength of the current SF episode differs drastically in these two galaxies, despite the fact that their ages are rather close, ∼3–3.8 Myr (see Sect. 5.4). From the numbers in columns 7 and 8 of Table 3 one can estimate that the relative B-band luminosity of the starburst ($L_{\rm burst}/L_{\rm disk}$) is lower in the west galaxy compared to that of the east galaxy by a factor of ∼8. The size of the bright 'Gaussian' component decreases systematically from U to I for both galaxies, that mainly reflects the wavelength dependence of the seeing during observations. However, there is also a systematic difference of this size between the east and west galaxies for each band. This indicates that the brightest knot of the west galaxy is more compact than that for the east galaxy.

In Figure 3 we present the radial distributions of colours in both objects. Again, the filled squares are used for the east galaxy, and the open ones for the west galaxy. Since the seeing for the U-band image is significantly larger than that for B-band, to derive the $(U-B)$ radial profile, we convolved the B image to the effective seeing of the U-band image (that is obtain the resulting FWHM for surrounding stars equal to that on the U image).

3.3. Hα map and equivalent width

Since our main goal is to derive in both galaxies the true colours of the LSB underlying components, comprised of an older stellar population, we need to examine the contribution of the ionized gas emission so as to subtract it properly. The effect of this contribution can be followed directly from observations, e.g., from the map of the value of EW(Hα). Since the equivalent width of the R-band filter is ∼1600 Å, an additional gas emission with EW(Hα) $\gtrsim$ 300–400 Å will result in a significant shift of the original colours of the underlying stellar population. For purely ionized hydrogen emission with $T_{\rm e}$ ∼20000 K the equivalent width EW(Hα)∼3500 Å (e.g., Aller 1984). So, even diluted radiation of the ionized gas can significantly alter the intrinsic colours of underlying stars.

To illustrate the importance of ionized gas emission, we show in Fig. 4 the images of both galaxies in the net Hα-line (with the line-free continuum subtracted) and the maps of distribution of EW(Hα), both in grey-scale and as isolines with the values of EW drawn. One can see that in the east galaxy the EWs of Hα in the outermost regions reach the level of 400–800 Å. In the west galaxy they are in general lower, and have the values of 100–200 Å. These diluted values of EWs show the relative contribution of the ionized gas emission and the stellar light in these regions to the R-band. Accounting for the R-filter transmission

(0.795) at Hα with the given galaxy redshift and the effective width of R-filter of ∼1600 Å, we estimate that in the east galaxy the nebular emission (Hα + continuum) will brighten the stellar continuum by $\sim 0\overset{m}{.}33$–$0\overset{m}{.}65$. In the west galaxy this brightening is $\sim 0\overset{m}{.}08$–$0\overset{m}{.}16$.

4. Models and evolutionary status

4.1. Method description

The observed light from an actively star-forming galaxy is a mix of the stellar and ionized gas radiation affected by the dust extinction inside the galaxy and in the Milky Way. The maximum portion of nebular emission emerges from the giant H II regions surrounding young stellar clusters often situated close to the central parts of star-forming galaxies. However, nebular emission can also significantly contribute to the light of the outer parts of some of blue compact galaxies. For this reason, in the analysis of stellar ages we can not directly use the results of the broad-band surface photometry. Instead, we need to take into account the possible contribution of nebular emission. To a first approximation, this can be done based on the intensity of Hα emission over the galaxy body and on the information on the radial trends of such parameters as electronic temperature and element abundances, derived from the long-slit spectroscopy results (here, from Izotov et al. 1999, 2001).

Thus, one of the necessary steps is the creation of the ionized gas nebular spectrum for each studied position of the galaxy image. This should be subtracted from the original broad-band fluxes at each point. This nebular spectrum consists of two parts. The first one is a purely recombination spectrum of hydrogen-helium plasma described, e.g., in Aller (1984). It includes lines of hydrogen, He I and He II (with the latter derived from the accepted ratios of $N(\mathrm{He}^+)/N(\mathrm{H}^+) = 0.078$ and $N(\mathrm{He}^{++})/N(\mathrm{H}^+) = 0.003$ (Aller 1984; Izotov 1999). The continuum includes hydrogen free-free, free-bound and the two-photon radiation, and the respective components from He I and He II. This contribution can be estimated accurately, given the observed flux in the Hα-line, if we know the ionized gas electron temperature $\mathrm{T_e}$ distribution.

The second part of the nebular emission is related to the contribution of the strong emission lines of oxygen [O II] λ3727, [O III] λλ4959,5007 and moderate lines of other ions (e.g., [Ne III] λ3868). This is more uncertain, since it depends on the possible small variations in element abundances and the gas temperature. The easiest way to account for nebular emission in these galaxies is to use the results of their long-slit spectroscopy for the maximal radial distances from the bright starburst. Unfortunately, such data are available for the east galaxy only for two position angles and for the west galaxy for one position angle (Izotov et al. 1997, 1999, 2001; Lipovetsky et al. 1999). Since the hypothesis of the circular symmetry of these galaxies is not too realistic, these long-slit results can be used only as a first approximation.

Since we are interested in the colours of the underlying low-surface brightness components, we examined the effect of nebular emission only for the outermost parts of both galaxies, where we can neglect the scattered light of bright starbursts. However, to have a sufficiently large signal-to-noise ratio in the studied regions, we are limited by the effective radii, which correspond to $\mu_\mathrm{B} \lesssim 25.5$ mag arcsec^{-1} for the east galaxy (R_eff ≈7.5″) and 25.2 mag arcsec^{-1} for the west one (R_eff ≈5″).

To minimize the effect of different seeings in various broad-band filters and in Hα on the derivation of the gas-free colours, we convolved the Hα image to the seeing of the respective broad-band image. This was performed before subtracting nebular the emission from U, B and V images. For R and I images the seeing was the same as for the Hα filter. However, due to the large difference between the seeing in the U-band image on the one hand, and in B-band and Hα-filter images, on the other hand, some systematic effects in the colour $(U-B)$ probably diminish the accuracy of our estimate of its gas-free part.

In our calculations of the nebular emission contribution we accepted the relative intensities of emission lines at respective radial distances (see Table 4) as derived from the 2D long-slit Keck telescope spectrum, kindly provided by Y.Izotov (Izotov et al. 2001). To account for the possible variations of the relative intensities on azimuth, we allowed that the average line intensities of strong lines in the ring can differ from those measured in some specific sector of the ring by as much as 5%. This is consistent with the maximal variations along the slit seen in the periphery of this galaxy. This uncertainty can result in additional errors of the gas-free colours of the level of 0.03 – 0.04 mag.

Thus, the estimates of the gas-free colours have been made on the regions with R_eff ≈7.5″ for the East galaxy and with R_eff ≈5″ for the West galaxy. To investigate the influence of gas electron temperature on the estimated stellar ages, we created two versions of the ionized gas spectra with T_e=15000 K and 20000 K. As shown by Izotov et al. (1999, 2001), the electron temperature within the supergiant H II region of SBS 0335-052 E has no significant gradient and remains in the range of T_e from 18000 to 23000 K. For the considered nebular emission, the electron temperature T_e was adopted to be of 20000 K. If it would be as low as 15000 K, the derived colours of the gas-free 'disk' would be at most 0.02 mag. bluer.

For each pixel we connected the intensities of the model nebular spectra (lines and continuum) with the observed Hα flux in the pixel, according to the relations from Aller (1984). Then the model nebular spectra were redshifted to z=0.0134, and convolved with the passband transmission curves of the U, B, V, R and I filters. The derived flux of nebular emission in each of the filters was subtracted from the fluxes of the respective original CCD images, corrected for Galactic extinction according to the Whitford (1958) law, pixel by pixel. For the resulting CCD images with subtracted nebular emission we built in each filter the SBPs of the gas-free light.

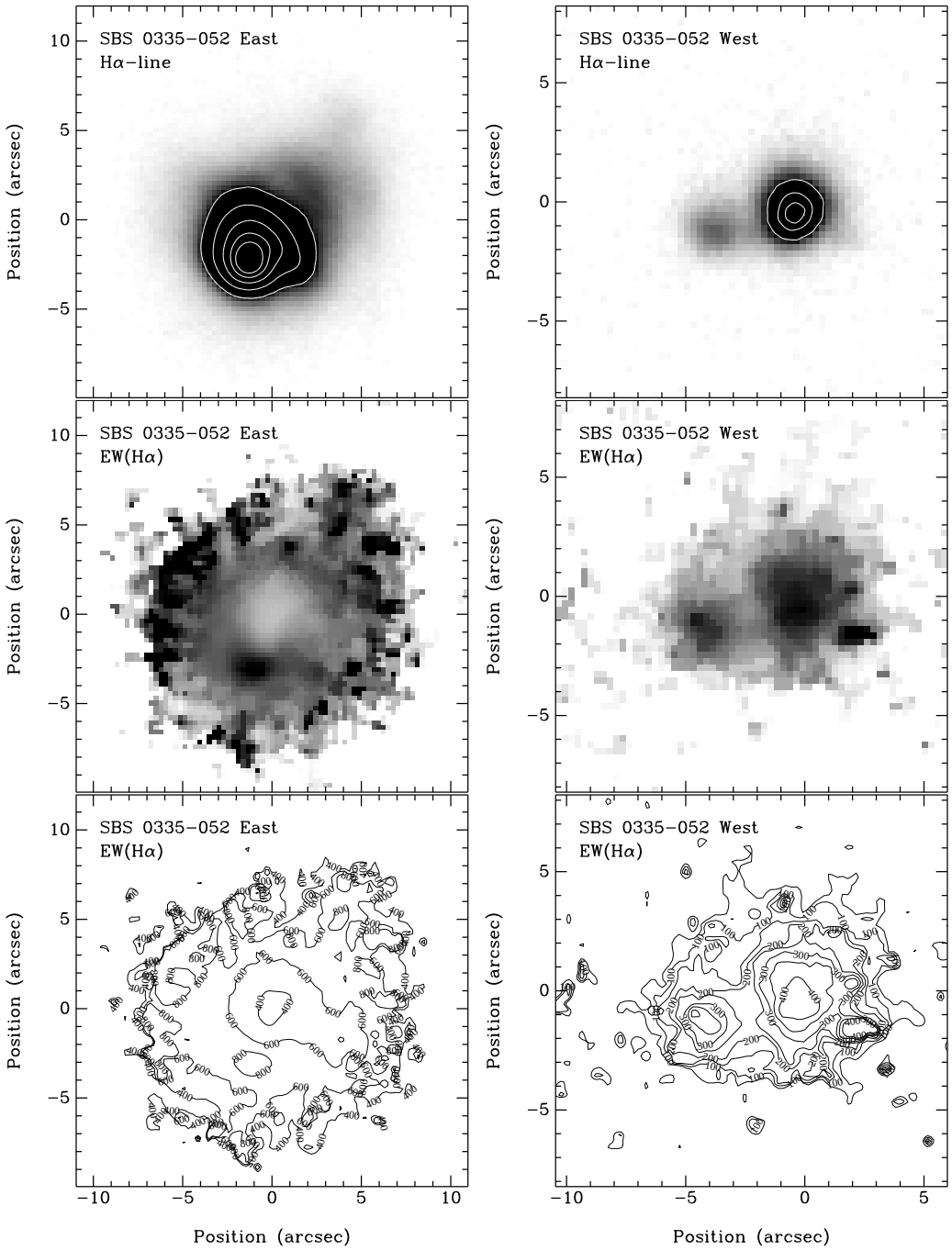

Fig. 4. From top to bottom: images of Hα-line flux, grey-scale and contour maps of EW(Hα) for galaxies SBS 0335–052 E and W. On each image grey-scale is normalized to the respective maximum value. Isophotes superimposed on Hα flux image correspond to the surface brightnesses 20.3, 20.7, 21.5, 22.5 and 23.5 mag arcsec^{-2} – for the east galaxy, and 23.2, 23.5 and 24.1 mag arcsec^{-2} – for the west galaxy.

The derived gas-free colours $(U-B), (B-V), (V-R)$ and $(R-I)$ at the respective $R_{\rm eff}$, corrected for the Galactic extinction, are summarized for both galaxies in the 3-d column of Table 5. The radial distributions of gas-free colour $(R-I)$, as the least model-dependent one, are shown in Fig. 3 (bottom-right panel). This gas-free colour is the most robust, since the nebular emission due to the strong Hα emission in the R-band is determined directly from observations, while in I-band the nebular continuum and He lines are also determined directly and the strong lines of other elements are absent. Possible variations in the fluxes of He I λ6678 and [S II] λ6716,6731 lines affect the R and I-band magnitudes by less than $0\overset{\rm m}{.}02$. While the original $(R-I)$ colours differ significantly, the gas-free ones are very close, and show only mild variations

Table 4. Adopted line intensities of the model spectra

λ_0(Å) Ion	I(λ)/I(Hβ)	λ_0(Å) Ion	I(λ)/I(Hβ)
3727 [O II]	0.43	4363 [O III]	0.05
3750 H12	0.03	4471 He I	0.04
3771 H11	0.04	4686 He II	0.03
3798 H10	0.05	4861 Hβ	1.00
3835 H9	0.07	4959 [O III]	0.50
3868 [Ne III]	0.30	5007 [O III]	1.50
3889 H8	0.11	5876 He I	0.06
3967 H7	0.25	6563 Hα	2.73
4101 Hδ	0.26	6678 He I	0.05
4340 Hγ	0.48	7065 He I	0.05

with radius, between −0.1 and 0.0 – for the W galaxy, and between −0.1 and +0.1 – for the E galaxy.

Since there is no reliable information on the dust distribution in the outermost parts of both the E and W galaxies, we did not include this in the procedure of gas-free colour estimates. If some small internal dust extinction is present ($E(B-V) \lesssim 0.20$, Izotov et al. 2001), its effect on the gas-free colours will depend on the mutual distribution of 'old' stars and the ionized gas. If the z scale for both components is close, they will be well mixed within the same volume, and the full effect of the extinction will be the same for gas and stars. In this case it will be equivalent to the additional Galactic extinction, and thus will have no effect on the resulting colours of the stellar population. If the ionized gas 'disk' is thicker than the stellar one, the value of the reddening of the stellar light will be somewhat higher than that of the gas. This difference, if present, will lead to bluer extinction-corrected colours and resulting younger ages of underlying stars. Since we ignore the possible internal extinction, the derived ages of old stellar populations are, in this aspect, also the upper limits of the real ages.

4.2. Models to estimate the ages of underlying populations

The derived $(U-B), (B-V), (V-R), (V-I)$ and $(R-I)$ colours of the underlying stellar population have been compared with the respective model colours from the PEGASE.2 package (Fioc & Rocca-Volmerange 2000). PEGASE.2 supersedes the previous version of the spectrophotometric evolution model for starbursts and evolved galaxies of the Hubble sequence (Fioc & Rocca-Volmerange 1997). The main differences of the new version are stellar evolutionary tracks with non-solar metallicities, the library of stellar spectra of Lejeune et al. (1997, 1998) and radiative transfer computations to model the extinction. The codes of PEGASE.2 take into account the evolutionary tracks of Girardi et al. (1996), Fagotto et al. (1994a, 1994b, 1994c) and Bressan et al. (1993). The models of Groenewegen & de Jong (1993) are used to compute the AGB and post-AGB phases.

For calculation of the model colours, we accept the metallicity $Z_\odot/50$ (the nearest of the available model parameters to the observed ones), the Salpeter (1955) IMF with M_{low} and M_{up} of 0.1 and 120 $M_\odot$, respectively. In Figure 5 we plot the calculated evolutionary tracks for the colours $(U-B), (B-V), (V-R), (R-I)$ and $(V-I)$. Three types of star formation scenarios are presented: instantaneous starburst, constant SFR and exponentially decreasing SFR with the e-fold time of τ=3 Gyr. The shadowed strips show the $\pm1\,\sigma$ ranges for the derived gas-free colours of the underlying stellar population of SBS 0335–052 E at $R_{\rm eff} = 7.5''$ (shown by horizontal lines in the middles of these strips). The observed colours of the underlying component (at $R_{\rm eff} = 7.5''$) of the E galaxy (corrected for the Galactic extinction) and corrected for nebular emission are presented in columns 2 and 3, respectively, in the upper half of Table 5. The respective allowable ages of the stellar populations for the three SF histories are presented in columns 4, 5 and 6 Table 5.

The similar data on the underlying component (at $R_{\rm eff} = 5''$) of the W galaxy are presented at the bottom of Table 5. In Figure 6, similar to Figure 5, the gas-free colours are shown with their uncertainties (shadowed strip), again compared to the same PEGASE.2 model tracks as for the east galaxy.

5. Discussion

5.1. Comparison of the derived colours with the previous analysis and age estimates

Since the age of the underlying stellar component in SBS 0335-052 E was the subject of some debate, we discuss this point in more detail. The $(U-B)$, $(B-R)$ and $(R-I)$ colours of the outermost regions of this galaxy were presented by Papaderos et al. (1998). These authors also compared their results with the colours of the evolving stellar population, based on the calculations performed in that work. They concluded that the colours of the east galaxy, after accounting for the nebular emission contribution, are consistent with the ages less than ∼100 Myr. However, Kunth & Östlin (2001) criticized that conclusion. They performed a comparison of the colours from Papaderos et al. (1998) with the more advanced model tracks, based on the PEGASE.2 package. From this they concluded that the same colours are best explained by the stellar population with the age of several Gyr.

While for comparison we also use the models based on the PEGAS.2 package, our results differ drastically from those by Kunth & Östlin (2001). The source of this discrepancy is the choice of colours of the underlying 'disk' component. In Sect. 3.2 (Figure 3) and in Table 5 (second column) we present our estimates of the colours in question. The latter correspond to those measured for the annulus with $R_{\rm eff} = 7\farcs5$. Those colours are consistent within the uncertainties with the colours of the LSB 'disk' derived as the respective differences of $m_{\rm disk}$ for various filters in Table 3 (after correction for the Galactic extinc-

Table 5. Ages of the underlying stellar populations in SBS 0335–052 E and W

Colour	Observed	Nebular emission excluded	Model stellar ages (Myr) Instantaneous	Continuous	Exponential $\tau = 3$ Gyr
East galaxy (at $R = 7\farcs5$)					
$U-B$	-0.89 ± 0.14	-0.86 ± 0.14	$4 \div 25$	$4 \div 120$	$4 \div 120$
$B-V$	0.20 ± 0.06	0.10 ± 0.07	$100 \div 350$	$400 \div 2000$	$400 \div 1500$
$V-R$	0.19 ± 0.07	0.17 ± 0.09	$100 \div 800$	$200 \div 6000$	$200 \div 3500$
$R-I$	-0.30 ± 0.11	0.08 ± 0.11	$14 \div 120$	$35 \div 400$	$35 \div 350$
West galaxy (at $R = 5\farcs0$)					
$U-B$	-0.39 ± 0.16	-0.39 ± 0.16	$45 \div 200$	> 350	$350 \div 3500$
$B-V$	-0.17 ± 0.11	-0.13 ± 0.11	$4 \div 60$	$4 \div 250$	$4 \div 250$
$V-R$	0.48 ± 0.11	0.49 ± 0.11	> 4000	> 10000	> 10000
$R-I$	-0.12 ± 0.13	-0.03 ± 0.13	$0 \div 70$	$0 \div 160$	$0 \div 150$

Ref: (1) – Data from this paper;

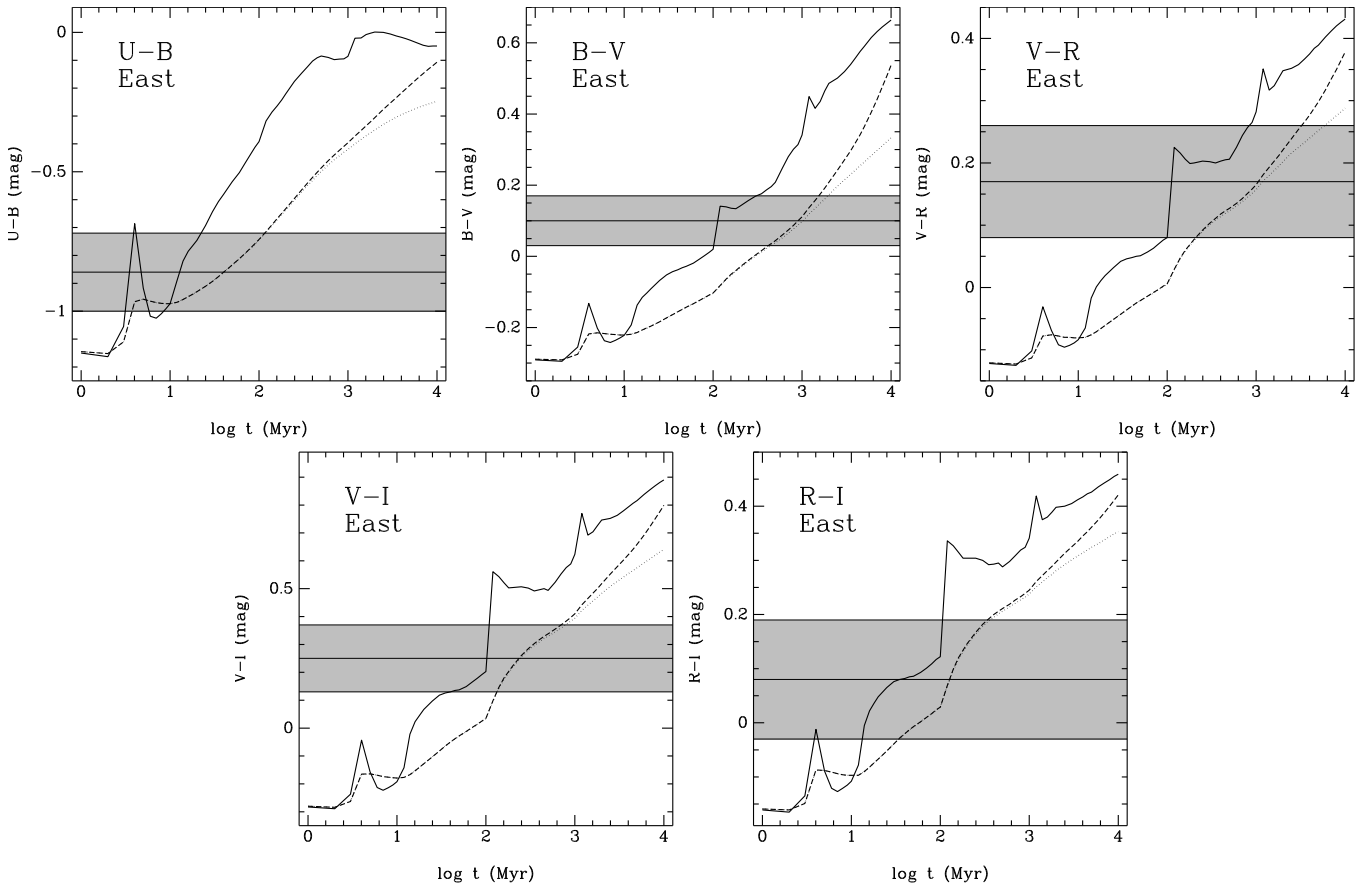

Fig. 5. PEGASE.2 model evolution tracks (see text for details). Solid line – instantaneous burst model, dotted line – constant star formation rate, dashed line – exponentially decreasing star formation rate with τ=3 Gyr. Horizontal lines show derived colours of the underlying LSB component of the east galaxy with nebular emission subtracted. Shadowed regions give the ranges of ± 1 σ uncertainties of the derived colours.

tion). Despite our *integrated* magnitudes and colours of this galaxy being more or less consistent with those from Papaderos et al. (1998), the colours of the 'disk' component in the periphery, as given in Table 3, differ somewhat. Our colours are significantly bluer. Therefore, even after the correction for nebular emission, they remain sufficiently blue. Hence, comparing these gas-free colours of the outermost regions with the same PEGASE.2 models as used by Kunth & Östlin (2001), we derive the ages of stars much lower compared to those derived by Kunth & Östlin (2001) from the colours of Papaderos et al. (1998).

As was noticed above, due to the poor seeing of the U-band image, our data on $(U-B)$ colours are less reliable. The east galaxy 'disk' appears too blue and is only

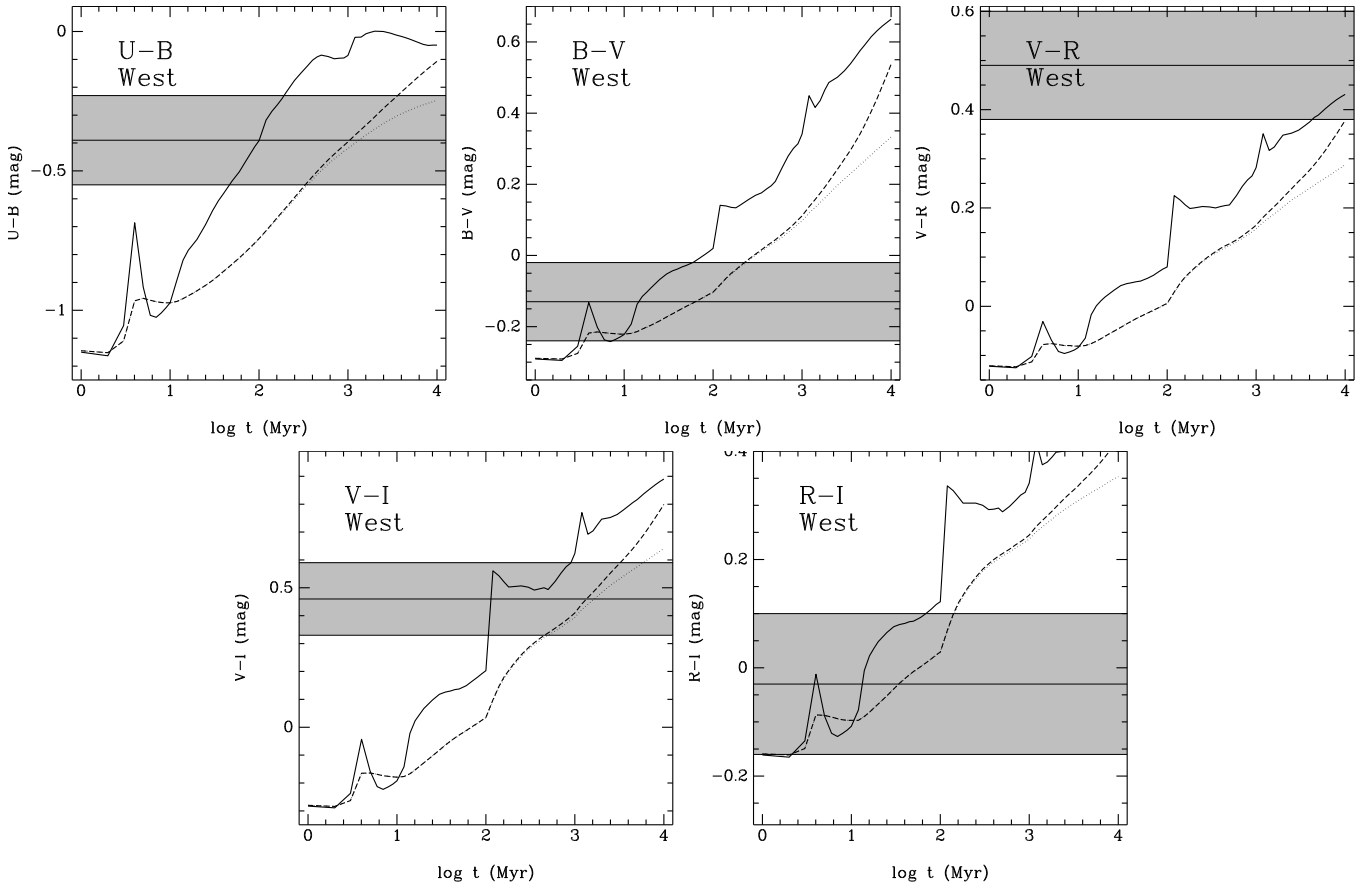

Fig. 6. PEGASE.2 model evolution tracks (see text for details). Solid line – instantaneous starburst model, dotted line – constant star formation rate, dashed line – exponentially decreasing SFR with τ=3 Gyr. Horizontal lines show derived colours of the underlying LSB component of the W galaxy with nebular emission subtracted. Shadowed strips show the limits of ± 1 σ uncertainties of the derived colours.

marginally compatible with the rest colours for continuous a SF history. For all other colours of gas-free emission, the best fit is reached for the instantaneous starburst with an age of ∼100 Myr. For continuous SF laws, different colours give less consistent ages. However, If such scenarios are considered as an alternative to the former model, they give the ages of $\lesssim$400 Myr. If we accept the $(U-B)$ radial distribution from Papaderos et al. (1998), as derived from the data with significantly better seeing, the compatibility of gas-free $(U-B)$ with other colours improves. Within the cited uncertainties the ages of the 'disk' stars derived from $(U-B)$ will fall roughly into the same range of less than a few hundred Myr, as for other gas-free colours.

Thus, applying the same models to the new colours of the SBS 0335–052 E 'disk' component, and directly accounting for the observed nebular emission contribution, we conclude that at the BCG periphery only the young population gives the detectable contribution to the light of this galaxy.

For the W galaxy there are no self-consistent gas-free colours, which could match those of a one-mode population (neither instantaneous nor continuous SF). All colours, besides $(V-R)$, are rather blue indicating instantaneous SF ages of $\lesssim$100 Myr, or a continuous SF with ages less than 200–300 Myr. $(V-R)$ is, however, too red, implying the minimal age of ∼4000 Myr. The reason for the significant inconsistency between $(V-R)$ and other colours is unclear.

The only reasonable explanation is related to the possible global error of the V-band zero-point calibration of the order of 0.1 magnitude. We have checked this option since the original total V-band magnitude of the east galaxy derived from the BTA image appeared $0\overset{\mathrm{m}}{.}2$ brighter than that from the HST measurement (Thuan et al. 1997). We additionally calibrated our V-band image taken with the Jacobus Kapteyn telescope (Canarias). Based on this calibration, we derived that the total V-band magnitude is closer to the HST value and shifted the zero-point of the BTA image. Despite the fact that this seems to be the most probable source of the systematic shift of V-band magnitude in the W galaxy, careful examination of this procedure did not reveal any sources of the error. Therefore we favor the colours of the underlying LSB component presented in Table 5.

5.2. Constraints on the contribution of old stars

The M/L ratio for the old low-mass stars is many times higher than that of a 100-Myr old 'disk' component. Therefore one can not exclude that there exists a substantial mass of a hidden old stellar population which has only a subtle contribution to the optical light of the 'disk'. To constrain its mass, we constructed the tracks on the colour-colour diagrams which describe composite colours of the mixtures of the 100-Myr 'young' SSC with the varying fraction of old stars (similar to the analysis in Pustilnik et al. 2003). The relative contribution of light in the broad-band filters for various mixtures was calculated based on the PEGASE.2 package. The comparison of the observed gas-free colours (with their uncertainties) with these tracks implies that a hidden 10-Gyr old population can have a mass no more than twice that of the mass of the 'young disk'.

In a similar manner, we compared the gas-free 'disk' colours with the model tracks for composite population, in which a 'young' component is defined as that with continuous SF over the last 400 Myr, while the old one is a result of continuous SF during the last 10 Gyr, as above. The mass of the hidden old stars should be less than one mass of the visible 400-Myr old population. This implies that if a 10-Gyr old population exists, the SFR related to this should be a factor of 25 lower than the average SFR during the last 400 Myr.

If we have in mind the hypothesis of merging (see Sect. 5.5), then the probable 1st close encounter (that occurred about 1 Gyr ago) might result in the trigger of an earlier SF episode, with an age of ∼0.5 Gyr. The latter case would be consistent with the alternative interpretation of the 'disk' colours as due to continuous SF during the last ∼400 Myr. The additional argument of the several hundred Myr age of the youngest XMD BCGs was suggested recently by Izotov et al. (2003) based on their characteristic value of $\log(\mathrm{N/O}) = -1.6$ compared to the lowest value observed in the damped Ly-α (DLA) systems of $\log(\mathrm{N/O}) = -2.3$.

5.3. Ionized hydrogen morphology

Quite poor seeing prevents us from resolving the compact starburst component of the east galaxy. However, our rather deep Hα-image allows us to follow the morphology of the ionized gas in the outermost low contrast regions. This is very irregular and filamentary. A very prominent arc is seen at ∼5″ NW the Hα brightness peak. At larger distances some filaments also emerge along this direction.

There is a small displacement of the maximum of Hα brightness (and EW(Hα)) for the east galaxy relative to the B-band brightness peak (Fig. 3). On the other hand, the brightness peaks of the east galaxy in all broad-band filters coincide within ∼0.″14. The same is valid for the W galaxy. The Hα peak in the east galaxy is displaced from that in B-band by 0.″34 to the East and 0.″56 to the South, a total of 0.″65 (or 167 pc). A similar displacement of the peaks in the distributions of continuum and strong lines in the long-slit spectra was noticed by Izotov et al. (1997, 1999). Most probably this is related to the complex structure of the region of current/recent star formation, as seen from the HST V-band image of Thuan et al. (1997). The total extent was ∼2″ along the direction SSE–NNW; it was resolved into six super-star clusters (SSCs) with ages from a few Myr to 25 Myr.

For the W galaxy, the position of the Hα peak coincides with that of the B-band within 0.″17, that is, the morphology of the ionized gas correlates rather well with that seen in the broad-band filters. This presumably indicates significantly lower age differences between the star-forming regions in the two components of the W galaxy.

5.4. SFR, stellar and gas masses

Having the Hα-luminosity of the studied galaxies, we could derive its SFR, following commonly used relations. But this is not of practical use. As shown by Weilbacher & Fritze-v.-Alvensleben (2001, hereafter WF01), the relation between Hα-luminosity and SFR in the blue compact galaxies is strongly time-dependent (on the time scale of a few Myr). This differs from the relations of Hunter & Gallagher (1986) or Kennicutt et al. (1994) derived for dIrr or spiral galaxies with more or less stationary star formation and metallicity near solar. For short intense starbursts taking place in low-metallicity BCGs, the SFR derived from Hα luminosity through the commonly used formula can result in an overestimation by a factor of >> 10 (WF01).

More important parameters are the total mass of stars formed during the current SF episode and the time elapsed since the beginning of this event. When the latter is known, the total mass of a starburst can be found using its total luminosity in broad bands and Balmer lines, through, e.g., the Starburst99 (SB99, Leitherer et al. 1999) or PEGASE.2 packages. Adopting the EWs of Hα and Hβ from Izotov et al. (1997, 1999) and Lipovetsky et al. (1999) for the east and west galaxies, respectively, we can estimate the age of instantaneous starbursts in these objects.

For the east galaxy, EW(Hβ)∼240 Å near the central region implies the age of a starburst with the Salpeter IMF (in the range between $M_{\rm low}$=0.8 and $M_{\rm up}$=120 $M_\odot$) of either ∼3 Myr or 3.7 Myr (Schaerer & Vacca 1998). Discovery of WR features in the brightest part of its spectrum (Izotov et al. 2001) corroborates this estimate, since the models predict the appearance of WR stars at such low metallicities only in the range of ages between ∼3 and ∼4 Myr (Schaerer & Vacca 1998). Then, for $m_{\rm burst}$=17.49 (from column 8 of Table 3) we get its absolute magnitude $M^{B,0}_{\rm burst} = -16.38$. Respectively, $M^{B,0}_{\rm disk} = -15.91$. From the PEGASE.2 models with the Salpeter IMF and $M_{\rm low}$ and $M_{\rm up}$ of 0.1 and 120 $M_\odot$, for the adopted starburst B-band luminosity and Z=$Z_\odot$/50, the mass of the current starburst ∼5.7×10^6 $M_\odot$. For the mass of the underlying disk, if it was formed in the instantaneous starburst ∼100 Myr ago, $M_{\rm disk}$∼4.2×10^7 $M_\odot$. For the alternative option

of the underlying disk formed continuously over the last 400 Myr, with the same IMF and Z, its mass would be $4.0\times10^7\ M_\odot$.

For the west galaxy the EW(Hβ)∼100 and 140 Å measured in the 2 knots (Lipovetsky et al. 1999) imply the larger age of recent starburst, ∼4 Myr. However, as follows from the comparison of the Hα flux measured here with that from Lipovetsky et al. (1999), about a half of all Hα flux is outside the region for which the EW(Hβ) was derived. This implies that the real EW(Hβ), which should be compared with the models, is about a factor of 2 higher. This, in turn, implies that the age of the recent SF episode in the W galaxy is also lower, ∼3.8 Myr. With the use of the same PEGASE.2 models, the masses of the recent starburst and the underlying older population are derived from the absolute blue magnitudes for the starburst and for the 'disk' in Table 3. They are $\sim1.3\times10^5\ M_\odot$ for the starburst and $\sim1.2\times10^7\ M_\odot$ for the 'disk' with the characteristic age of ∼100 Myr. The total visible masses of stars in the east and west galaxies differ by a factor of ∼4. For the option of the 'disk' with continuous SF during the last ∼400 Myr the underlying disk mass of the W galaxy would be of $\sim1.25\times10^7\ M_\odot$.

The gas or stellar mass-fractions are important parameters in models of chemical evolution. We address this issue below. If we consider the H I mass for each of the galaxies separately, then the mass of neutral gas related to each of them is ∼1.0 and 1.1 $\times10^9\ M_\odot$ (Pustilnik et al. 2001a).

The mass of the ionized gas in the east and west galaxies can be roughly estimated from their total Hα luminosities, assuming the gas spatial distribution. For 'disk' fractions of both galaxies we assumed the scaleheight to be close to their scalelengths. For the 'Gaussian' component in the east galaxy we assumed a radial distribution with the characteristic radius from Table 3. With these inputs we estimate the ionized gas mass as $2.5\times10^8\ M_\odot$ for the east galaxy and $2.4\times10^7\ M_\odot$ for the west galaxy.

The mass fraction of visible stars in the east galaxy comprises ∼0.035 of the total baryon mass, while in the west galaxy this is only ∼0.011, implying rather different SF histories. For the option of the underlying 'disks' with the age of ∼400 Myr, the mass fractions of stars will be close to the above values. We emphasize also other important differences in the properties of these two galaxies. As noticed in Sect. 3.2, while the ages of current starbursts are very close, their relative strengths differ by a factor of 8. The significant difference in their central surface brightnesses indicates an intrinsic difference in their mass distribution and/or SF history.

5.5. SBS 0335–052 system as a representative of the merger evolution sequence

As was discussed, e.g., by Pustilnik et al. (2001a), there are two scenarios resulting in such an unusual pair of dwarf galaxies. The first one is related to a unique retarded protogalaxy, a kind of free-flying H I cloud, which could appear as a local Ly-α absorbing cloud (e.g., Manning 2002, 2003). This large neutral gas cloud finally reached outskirts of the loose group LGG 103 and experienced sufficiently strong tidal disturbance from the giant spiral NGC 1376 (at a projected distance of ∼150 kpc). Resulting gas collapse and star formation occurred recently in two off-center positions roughly symmetric relative to the cloud center. They appear now as two young galaxies immersed in the single disturbed H I cloud.

The second scenario considers two very gas-rich objects with similar gas mass (either purely gas clouds, or very slow evolving galaxies, as expected for very low SB galaxies) currently seen in H I morphology to be in contact. Their recent collision and the consequent merging caused strong disturbance and the loss of gas stability in each of them (see, e.g., simulations in Springel (2000) and references therein). Gas infall to the component centers with subsequent collapse caused the onset of the first or the additional enhanced star formation.

The very significant difference in the optical properties of the east and west galaxies, discussed above, suggests that these two objects are intrinsically very different and, hence, favors the second scenario. We discuss this option in more detail and follow possible interrelations of SBS 0335–052 with other XMD galaxies.

One of the main objections for the collision/merging scenario is very small probability of such an event, given the estimates of the density of such objects. The argument which completely diminishes this difficulty is the existence of another similar system. This is well known Dw 1225+0152, the optical counterpart of the giant H I cloud HI 1225+01 with $Z\sim Z_\odot/20$ studied in detail by Salzer et al. (1991) and Chengalur et al. (1995). This H I cloud consists of two separate components with about the same mass ($\sim10^9\ M_\odot$) at a distance of ∼2 visible diameters of these two H I components, joined by tidal bridge. While in the NE component we observe a star-bursting dwarf galaxy, the SW component shows lack of detectable optical emission down to a V-band surface brightness of 27.0 mag arcsec^{-2} (Salzer et al. 1991). The SW component is thus either a purely gas object, or an extremely low surface brightness galaxy. The stability of gas in the SW component is significantly higher than for the NE one, since the current SF rates in both objects differ drastically, while their tidal disturbances are comparable.

Comparing the H I morphology and velocity field of this object with the N-body simulations (Barnes & Hernquist 1991), Chengalur et al. (1995) argue that these objects have recently experienced the first close encounter, and during the next one the system will merge. Consequently, while the merging of the two components will progress, one can expect that the stronger disturbance will cause the gas collapse in the SW component and trigger its star formation. This seems to resemble the current situation in the SBS 0335–052 system, where we see strong starburst in the east component, and quite a modest SF event in the west component. One more similarity of these

two systems is their belonging to low-density outskirts of galaxy aggregates. The distance to Dw 1225+0152 is somewhat uncertain due to the complications with the distance estimates in the vicinity of the Virgo cluster. However, it is quite probable that it is situated at the distant periphery of this cluster.

If this is the case, the existence of both systems implies that in the near environment of various bound galaxy aggregates (or more exactly, in some fraction of them) there exists an abundant population of very gas-rich objects with masses of the order of 10^9 $M_\odot$. Presumably, such galaxy aggregates are quite rare, since searches for H I clouds in the Local Volume and some nearby groups with the mass detection limit of 10^7–10^8 $M_\odot$ gave only a few detections (e.g., Henning & Kerr 1989, Putman et al. 1998).

If this scheme is correct, then SBS 0335–052 and Dw 1225+0152 can be considered as an evolution sequence along with two other recently discovered XMD blue compact galaxies: HS 0822+3542 ($Z \sim Z_\odot/30$, Kniazev et al. 2000b) and HS 0837+4717 ($Z \sim Z_\odot/20$, Kniazev et al. 2000a). HS 0822+3542 is a member of a binary gas-rich galaxy system with a very small relative velocity and projection distance of 11 kpc, or ∼4 components' H I diameters (Pustilnik et al. 2003, Chengalur et al. 2004). The mass and luminosity of the second component are comparable to those of the BCG, but its surface brightness and SF are typical of LSB dwarfs. This system can be considered as a pre-merger, preceding the stage observed in HI 1225+01 system.

HS 0837+4717 seems a very probable well advanced merger, with a disturbed morphology and gas velocity field. Two knots near the object center are separated by only ∼2 kpc (Pustilnik et al. 2004). In the suggested scheme, the case of HS 0837+4717 can be treated as a well advanced system of SBS 0335–052. Two more XMD galaxies – HS 0122+0743 and HS 2236+1344, found in HSS-LM (Ugryumov et al. 2003) also support the merger scenario. It is too early to estimate the fraction of mergers among XMD BCGs. However, it is worth noting that the H I morphology and kinematics of a prototypic XMD galaxy I Zw18 (van Zee et al. 1998) suggest a possible recent interaction/merger in this system. This scenario can be examined more carefully by comparing all available observational data with N-body simulations of low-mass gas-rich (proto)galaxy mergers.

Such an evolutionary scheme does not imply the tight correlation of metallicity with the merger phase, since it can invoke a rather wide range of very low metallicities of pre-merger objects. However, on average, the objects representing almost complete mergers should be more metal-enriched due to the intense SF accompanying the merger at the final stage.

Within the merger scenario some additional implications can be made for SBS 0335–052 system itself. If this is a well-advanced merger, presumably at the stage of the second (and the last) encounter, some interesting consequences should exist of the first encounter, similar to that seen in the system HI 1225+01. Following the analogy between these two systems, we could expect that during the first encounter the significant tidal disturbance ignited some SF in the E component, which is characterized by a higher surface brightness of the underlying 'disk'. In Sect. 5.2 we estimate the mass of stars formed in this SF episode.

One problem with such a scenario is the observed close metallicity of gas in the two merging dwarfs. This likely can be explained by the significant exchange of gas between the two components during the first encounter (e.g., Mihos & Hernquist 1996) and the following mixing, which should result in similar metallicities. The best way to better constrain when the first episode of star formation took place and how much gas mass was transformed into stars is to study the colour-magnitude diagram of individual resolved stars on the galaxy periphery. In such a scenario, if the east galaxy is truly young, the west galaxy also should be young, since this is even more stable relative to the external perturbations.

6. Summary and conclusions

In this work we have analyzed the results of the 6-m telescope $UBVRI$ and Hα surface photometry of two extremely metal-deficient gas-rich galaxies SBS 0335–052 E and W. They represent a unique galaxy pair, both components of which show the properties of candidate young galaxies. We subtract the nebular emission, using their Hα-line intensity maps and the additional data on the spectra of the ionized gas. This gives us the gas-free colours of the underlying stellar population outside the regions of the current star-formation bursts. These colours are significantly bluer than those claimed in earlier works. These gas-free colours are compared with various PEGASE.2 evolution model tracks. The most self-consistent estimates of the ages of underlying stars do not contradict the hypothesis of youth of both galaxies.

The evidence for the importance of galaxy interactions and mergers, in particular, for the star-forming activity in BCGs was presented, e.g., by Pustilnik et al. (2001b). The arguments for the merger nature of luminous BCGs were presented by Bergvall & Östlin (2002, and references therein). In this aspect, XMD galaxies with SF bursts show similarity to the majority of more typical BCGs. A significant fraction of SF bursts in these galaxies are triggered due to strong disturbance from the other galaxy (or protogalaxy).

We draw the following conclusions:

1. The total magnitudes of new deep $UBVRI$ photometry of SBS 0335–052 E are consistent with the earlier data from Papaderos et al. (1998). This gives additional confidence in the new data for the Western galaxy derived from the same CCD frames. The only possible exception is its suspicious V-band zero-point.
2. The colours of the outer regions for the Eastern galaxy, derived in this work, however, are significantly bluer

than those claimed in earlier works. Similarly, our $(U-B)$ and $(R-I)$ colours of the outer regions of the Western galaxy are also significantly bluer than those from earlier studies.

3. The gas-free colours of the outer regions in the Eastern galaxy are derived with the use of the Hα-intensity maps. Compared to the evolution models of stellar populations from PEGASE.2, they are consistent (except for the more uncertain $(U-B)$ colour) with the ages of $\lesssim$100 Myr for instantaneous starburst. For a less consistent but still acceptable option – a scenario with continuous SF, the duration of this SF episode would be $\lesssim$400 Myr. For the underlying disk with an age of $\lesssim$100 Myr, the mass of a 10-Gyr old stellar population cannot exceed twice that inferred for the young disk stellar population. If, however, the disk was forming during the last $\lesssim$400 Myr, the mass of the hidden 10-Gyr old population would be less than or equal to that of the young stellar disk.
4. For the gas-free colours of the outer regions of the W galaxy, according to the data obtained the conclusions are less certain. The fully self-consistent combination of colours, matching the model colours of a stellar population with a unique SF history, is absent. However, 3 of the 4 independent colours are consistent with an instantaneous SF burst with an age of ∼70 Myr. Similarly, for the less consistent case of continuous SF, 3 of 4 colours indicate a period of star formation less than 200–300 Myr.
5. Star-forming properties and the central surface brightnesses of the E and W galaxies differ drastically, suggesting that the two galaxies are intrinsically very different. This, in turn, favors the hypothesis of the collision of two gas-rich XMD galaxies/protogalaxies.
6. We suggest an evolutionary scheme in which the systems HS 0822+3542/SAO 0822+3545, HI 1225+01, SBS 0335–052 and HS 0837+4717 comprise the sequence of XMD gas-rich objects at various stages of merging (from pre-merger to full merger). The interaction-induced SF in XMD gas-rich galaxies seems to be an important channel of their SF bursts.

Acknowledgements. The authors thank A.Kopylov for the help in observations. We are grateful to Y.Izotov who provided the deep long-slit Keck telescope spectrum of SBS 0335–052E, used in this work as a reference to model ionized gas emission. We are thankful to Y.Izotov for the fruitful discussion and useful notes on the preliminary version of the paper. The authors acknowledge the useful suggestions made by the anonymous referee, that allowed them to improve the presentation. The work was partly supported by the Russian Federal program "Astronomy". This research has made use of the NASA/IPAC Extragalactic Database (NED) which is operated by the Jet Propulsion Laboratory, California Institute of Technology, under contract with the National Aeronautics and Space Administration.

Table 6. Main parameters of galaxies SBS 0335–052 E and W

Parameter	0335−052 E	0335−052 W	Ref
α_{2000}	$03^{\rm h}37^{\rm m}44\overset{\rm s}{.}03$	$03^{\rm h}37^{\rm m}38\overset{\rm s}{.}40$	
δ_{2000}	$-05^\circ02'38\overset{''}{.}8$	$-05^\circ02'36\overset{''}{.}4$	
$B_{\rm tot}$ [mag]	16.95 ± 0.03	19.14 ± 0.03	5
$V_{\rm hel}$ [km s^{-1}]	4057	4017	2
D [Mpc]	54.3	54.3	1
$A_{\rm B}$ (NED)	0.20	0.20	
$M^0_{\rm B}$ [mag]	−16.92	−14.73	5
Size [arcsec]	23×20	14×14	3
12+log(O/H) [dex]	7.29	7.22	4
$T_{\rm e}$(O III) [K]	20290	17200	4
M(H I)[$\times 10^9 M_\odot$]	0.80	0.89	2
M(H I)/$L_{\rm B}$ [$M_\odot/L_\odot$]	0.9	7.3	5

(1) – Papaderos et al. (1998); (2) – Pustilnik et al. (2001a); (3) – maximal extent on B isophote 27.5 mag arcsec^{-2} from Papaderos et al. (1998) and this work; (4) – Izotov et al. (1999) for the Eastern and Lipovetsky et al. (1999) for the Western galaxy; (5) – this work.

References

Aller, L. H. 1984, in Physics of Thermal Gaseous Nebulae, Reidel, Dordrecht
Anders, E., & Grevesse, N. 1989, Geochim. Cosmochim. Acta, 53, 197
Barnes, J.E., & Hernquist, L.E. 1991, ApJ, 370, L65
Bergvall, N. & Östlin, G. 2002, A&A, 390, 891
Bessell, M. S. 1990, PASP, 102, 1181
Bohlin, R. C. 1996, AJ, 111, 1743
Bressan, A., Fagotto, F., Bertelli, G., & Chiosi, C. 1993, A&AS, 100, 647
Chengalur, J.N., Giovanelli, R., & Haynes, M.P. 1995, AJ, 109, 2415
Chengalur, J., Pustilnik, S.A., Martin, J.-M., & Kniazev, A.Y. 2004, A&A, in preparation
Fagotto, F., Bressan, A., Bertelli, G., & Chiosi, C. 1994, A&AS, 104, 365
Fagotto, F., Bressan, A., Bertelli, G., & Chiosi, C. 1994, A&AS, 105, 29
Fagotto, F., Bressan, A., Bertelli, G., & Chiosi, C. 1994, A&AS, 105, 39
Fioc, M. & Rocca-Volmerange, B. 1997, A&A, 326, 950
Fioc, M. & Rocca-Volmerange, B. 2000, [astro-ph/9912179]
Fricke, K.J., Izotov, Y.I., Papaderos, P., Guseva, N.G., & Thuan, T.X. 2001, AJ, 121, 169
Girardi, L., Bressan, A., Chiosi, C., Bertelli, G., & Nasi, E. 1996, A&AS, 117, 113
Groenewegen, M. A. T. & de Jong, T. 1993, A&A, 267, 410
Guseva, N.G., Izotov, Y.I., Papaderos, P., et al. 2001, A&A, 378, 756
Henning, P.A., & Kerr, F.J., 1989, ApJ, 347, L1
Hunt, L.K., Vanzi, L. & Thuan, T.X. 2001, A&A, 377, 66
Hunter, D.A. 1997, PASP, 109, 937
Hunter, D.A. & Gallagher, J.S. 1986, PASP, 98, 5
Izotov, Y.I., & Thuan, T.X. 1999, ApJ, 511, 639
Izotov, Y.I., Lipovetsky, V.A., Guseva, N.G., Kniazev, A.Y., & Stepanian, J.A. 1990, Nature, 343, 238
Izotov, Y. I., Lipovetsky, V. A., Chaffee, F. H., et al. 1997, ApJ, 476, 698

Izotov, Y. I., Chaffee, F. H., Foltz, et al. 1999, ApJ, 527, 757
Izotov, Y. I., Chaffee, F. H., & Schaerer, D. 2001, A&A, 378, L45
Izotov, Y.I., Stasinska, G., Guseva, N.G. & Thuan, T.X. 2003, A&A, in press = astro-ph/0311564
Kennicutt, R.C., Tamblyn, P., & Congdon, C.E., 1994, ApJ, 435, 22
Kniazev, A.Y., & Shergin, V.S. 1995, SAO RAS internal report No. 249, 1
Kniazev, A.Y., Pustilnik, S.A., Ugryumov, A.V., & Kniazeva, T.F. 2000a, Astronomy Letters, 26, 129
Kniazev, A.Y., Pustilnik, S.A., Masegosa, J., et al. 2000b, A&A, 357, 101
Kunth, D., & Östlin, G. 2001, A&SS Suppl. 277, 281
Landolt, A. U. 1992, AJ, 104, 340
Leitherer, C., Schaerer, D., Goldader, J.D., et al., 1999, ApJS, 123, 3
Lejeune, T., Cuisinier, F., & Buser, R. 1997, A&AS, 125, 229
Lejeune, T., Cuisinier, F., & Buser, R. 1998, A&AS, 130, 65
Lipovetsky, V. A., Chaffee, F. H., Izotov, Y. I., et al. 1999, ApJ, 519, 177
Manning, C. 2002, ApJ, 574, 599
Manning, C. 2003, ApJ, 595, 19
Melbourne, J., & Salzer, J.J. 2002, AJ, 123, 2302
Melnick, J., Heydari-Malayeri, M., & Leisy, P. 1992, A&A, 253, 16
Mihos, C., & Hernquist, L. 1996, ApJ, 464, 641
Papaderos, P., Izotov, Y. I., Fricke, K. J., Thuan, T. X., & Guseva, N. G. 1998, A&A, 338, 43
Papaderos, P., Fricke, K. J., Thuan, T.X., Izotov, Y.I., & Nicklas, H. 1999, A&A, 352, L57
Papaderos, P., Izotov, Y. I., Thuan, T.X., et al. 2002, A&A, 393, 461
Prieto, C.A., Lambert, D.L., & Asplund, M., 2001, ApJL, 556, 63L
Pustilnik, S.A., Lipovetsky, V.A., Izotov, Y.I., et al. 1997, Astronomy Letters, 23, 308
Pustilnik, S. A., Brinks, E., Thuan, T. X., Lipovetsky, V. A., & Izotov, Y. I. 2001a, AJ, 121, 1413
Pustilnik, S.A., Kniazev, A.Y., Lipovetsky, V.A., Ugryumov, A.V. 2001b, A&A, 373, 24
Pustilnik, S.A., Kniazev, A.Y., Pramskij, A.G., Ugryumov A.V., & Masegosa J. 2003, A&A, 409, 917
Pustilnik, S.A., Kniazev, A.Y., Pramskij, A.G., et al. 2004, A&A, 419, 469
Putman, M.E., Bureau, M., Mould, J.R., Staveley-Smith, L., & Freeman, K. 1998, AJ, 115, 2345
Salpeter, E. E. 1955, ApJ, 121, 161
Salzer, J.J., Di Serego Alighieri, S., Matteucci, F., Giovanelli, R., & Haynes, M. 1991, AJ, 101, 1258
Schaerer, D. & Vacca, W.D. 1998, ApJ, 497, 618
Springel, V. 2000, MNRAS, 312, 859
Thuan, T. X., & Izotov, Y. I. 1997, ApJ, 489, 623
Thuan, T. X., Izotov, Y. I., & Lipovetsky, V. A. 1997, ApJ, 477, 661
Ugryumov, A.V., Engels, D., Pustilnik, S.A., et al. 2003, A&A, 397, 463
van Zee, L., Westpfahl, D., Haynes, M., & Salzer, J.J. 1998, AJ, 115, 1000
Vanzi, L., Hunt L.K., Thuan, T.X., & Izotov, Y.I. 2000, A&A, 363, 493
Weilbacher, P.M., & Fritze-v. Alvensleben, U. 2001, A&A, 373, L9
Whitford, A.E. 1958, AJ, 63, 201